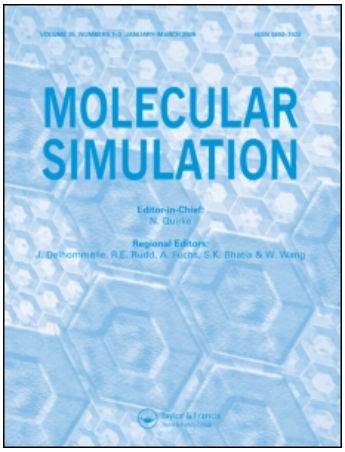

Molecular Simulation
Publication details, including instructions for authors and subscription information:
http://www.informaworld.com/smpp/title~content=t713644482

On the behaviour of fluidic material at molecular dynamics boundary conditions used in hybrid molecular-continuum simulations

M. Kalweit[a]; D. Drikakis[a]
[a] Fluid Mechanics and Computational Science Group, Department of Aerospace Sciences, Cranfield University, Cranfield, Bedfordshire, UK

Online publication date: 16 August 2010

To cite this Article Kalweit, M. and Drikakis, D.(2010) 'On the behaviour of fluidic material at molecular dynamics boundary conditions used in hybrid molecular-continuum simulations', Molecular Simulation, 36: 9, 657 — 662
To link to this Article: DOI: 10.1080/08927021003699799
URL: http://dx.doi.org/10.1080/08927021003699799

Molecular Simulation
Vol. 36, No. 9, August 2010, 657–662

Taylor & Francis
Taylor & Francis Group

On the behaviour of fluidic material at molecular dynamics boundary conditions used in hybrid molecular-continuum simulations

M. Kalweit and D. Drikakis*

Fluid Mechanics and Computational Science Group, Department of Aerospace Sciences, Cranfield University, Cranfield, Bedfordshire MK43 0AL, UK

(*Received 23 September 2009; final version received 14 February 2010*)

This paper presents an investigation of the behaviour of the density profile of fluidic material confined by a force field, as it occurs across molecular-continuum mechanics boundaries in multiscale, hybrid molecular-continuum simulations. A theoretical model for the density profile across the boundary is derived. Furthermore, numerical experiments to validate the density profile and thickness of the relaxation zone are performed using molecular dynamics for a Lennard-Jones fluid in gaseous, liquid and supercritical state conditions. The simulation results show excellent agreement with the theoretical model.

Keywords: molecular dynamics; boundary conditions; hybrid; density profile; interface

1. Introduction

When fluidic material is confined by a force field, a relaxation zone forms on the boundary, within which the density reduces from its bulk value to zero (vacuum). This zone has its origin in the different energy levels of the fluidic particles. Examples can be found in many areas of physics, ranging from the interstellar gas clouds, our planet's atmosphere to confinement of plasma. Another area where the confinement of fluids through external force fields becomes increasingly important is in molecular dynamics (MD) simulations [1] and multiscale modelling [9]. Historically, MD simulations have been performed with simple periodic boundary conditions, but, more recently, the need for more sophisticated boundary conditions, e.g. flux boundary conditions, has emerged due to a number of applications, including micro/nanofluidic devices, microsensors, micromixing and coating [5]. In many of these applications, non-equilibrium MD simulations, where the molecular system is non-periodic, need to be performed. Additionally, coupling of MD simulations with computational fluid dynamics (CFD) methods [6,9] is often considered. The need for coupling MD with CFD has arisen due to the deficiencies of molecular and continuum simulation methods: the continuum model is no longer valid when advancing towards microscopic and nanoscopic length scales, while molecular simulations are computationally expensive, thus their application is limited to relatively small systems.

The molecular domain used in the hybrid MD-CFD methods is usually finite and non-periodic with boundary conditions determined by the CFD solver. The way the boundary conditions are imposed differs significantly between individual coupling schemes and depends particularly on the kind of variables that the coupling concerns. Simple schemes couple only the static pressure and velocities and do not allow advection of the mass flux across the boundary [7]. More advanced methods aim to couple the full set of conservative variables of the Navier–Stokes equations [2,11]. These have also been applied to water [3] and used in conjunction with hydrodynamic fluctuations to reproduce the natural functions of the molecular system within the continuum domain [6]. Nevertheless, most coupling schemes impose the static pressure through an external force. The force mimics the effect of the atoms outside the molecular domain, which are not included in the simulation. To this end, a number of atoms on the boundary (boundary atoms) are selected onto which the external force is acting on. If an atom approaches the boundary, it is subjected to the external force and its velocity vector, which points originally outwards of the molecular domain, is gradually reversed. Since different atoms carry different amounts of kinetic energy, they move with different speeds through the molecular domain, thus leading to the emergence of a relaxation zone.

The relaxation zone plays an important role in the boundary conditions, because as the density changes the physical properties of the material, e.g. viscosity, change too. Ideally, one would like to achieve uniformity of the bulk fluid properties up to the edge of the MD computational domain. However, this is not achievable when the static pressure on the fluid is modelled through

*Corresponding author. Email: d.drikakis@cranfield.ac.uk

ISSN 0892-7022 print/ISSN 1029-0435 online

DOI: 10.1080/08927021003699799
http://www.informaworld.com

an external force because there will always be a relaxation zone. For an accurate MD-CFD coupling, the physically correct implementation of the MD boundary conditions is needed. It is, therefore, important to know the characteristics of the relaxation zone, including the width and density profile across the boundary. These are determined by a number of factors:

(a) the type of the fluid and specific properties, in particular the molecular size, surface tension, etc.;
(b) the state of the material, for example the density and temperature at the boundary; and
(c) the way the external force is distributed on the boundary atoms.

This paper focuses on (b) and (c). The general Lennard-Jones (LJ) potential [1] is employed to model the fluidic material and it is reasonable to expect that the findings reported in this paper also hold for other simple fluids. In respect of (c), previous coupling schemes [7] used a weighting function to distribute the external force in a way that the strength of the force is reduced asymptotically with the distance of an atom from the boundary. However, Delgado-Buscalioni and Coveney [2] pointed out that the simplest weighting function, according to which the external force is applied equally to a number of boundary atoms, has the advantage that, along with the force, the correct amount of energy is transferred too. With this distribution, the only parameter to select is the number of boundary atoms onto which the external force is applied to. This raises the questions of how many boundary atoms should be used and what effect this choice has on the density profile at the boundary. Clearly, this choice has a profound effect on the density profile of the fluidic material at the boundary. Distributing the external force over too many boundary atoms would result in a large diffusive zone. On the other hand, the application of the external force to a small number of boundary atoms would accelerate them strongly to high velocities leading to artefacts.

In this paper, an investigation of the influence of the number of boundary atoms onto the density profile across the relaxation zone for three different states of matter, gaseous, liquid and supercritical, is presented. MD simulations for a LJ fluid are performed with a force equally distributed onto the boundary atoms. The simulation results are presented in Section 3 and compared with a theoretical model for the density profile and the relaxation zone thickness, which is derived in Section 2.

2. Methodology

2.1 Molecular dynamics

The MD method is a deterministic simulation method based on the classical molecular model [1,5]. Atoms are modelled as point masses whose motion is governed by Newton's equation of motion: $\mathrm{d}^2(m_i\mathbf{r}_i)/\mathrm{d}t^2 = \mathbf{f}_i$, where $\mathbf{r}_i$ is the position of an atom i with the mass m_i and $\mathbf{f}_i$ is the force acting on it. The system's potential energy, $\mathcal{V}$, is the sum of the potential energies of all atoms of the system: $\mathcal{V} = \sum_i \mathcal{V}_i$ and the force on an atom i is $\mathbf{f}_i = -\nabla_{\mathbf{r}_i}\mathcal{V}_i$. The total energy of the system is given by $E_{\mathrm{tot}} = \mathcal{V} + \sum_i (1/2) m_i \mathbf{v}_i^2$. The atomic trajectories can be calculated by using a numerical time integration method. In this work, the LJ potential for modelling the pairwise atomic interaction has been used. The LJ potential between two atoms i and j is given by $\mathcal{V}^{\mathrm{LJ}}(r_{ij}) = 4\varepsilon[(\sigma/r_{ij})^{12} - (\sigma/r_{ij})^6]$, where the parameters ε and σ can be chosen to model a number of simple atomic substances [1]. All variable and parameter values throughout this paper are given in the reduced LJ units, which are based on ε, σ and the atomic mass, m_{a}: length $r \rightarrow r\sigma$; energy (and, similarly, temperature) $e \rightarrow e\varepsilon$; time $t \rightarrow t\sigma\sqrt{m_{\mathrm{a}}/\varepsilon}$; and velocity $v \rightarrow t\sqrt{\varepsilon/m_{\mathrm{a}}}$.

The large-scale atomic/molecular massively parallel simulator code developed at Sandia laboratories [10] was employed in the present study.

2.2 Definitions and relaxation zone model

An illustration of the relaxation zone is displayed in Figure 1. The static pressure that keeps the atoms inside the molecular domain is realised by the external force F^{ext}, acting to the right onto the N_{b} outermost atoms. Essentially, this force introduces a constant momentum flux into the system. For the static case, where the momentum transferred across the boundary with a surface area A_{b} is solely determined by the static pressure p, the external force is given by $F^{\mathrm{ext}} = pA_{\mathrm{b}}$. The width

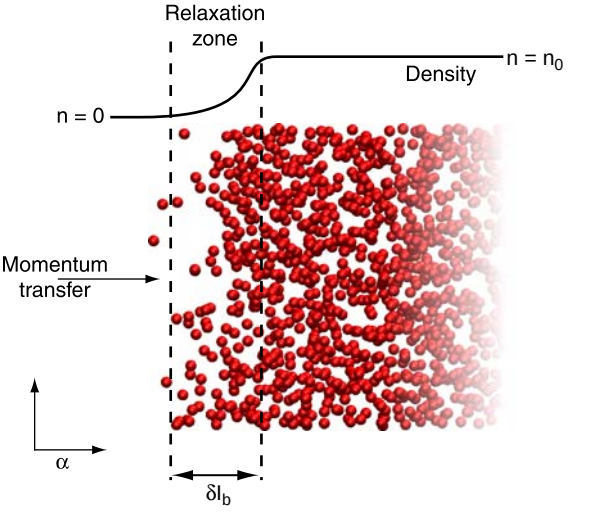

Figure 1. Illustration of the relaxation zone; the static pressure is applied through a momentum transfer in direction α onto the molecular system. The number density profile is indicated on the top.

(or thickness) of the relaxation zone is designated by δl_b. The density function across the zone shows an asymptotic behaviour. A criterion similar to that used for the definition of the thickness of shock waves was employed to define the thickness of the density transition zone between the two boundary values. According to this criterion, the relaxation zone ranges from $n = 0.05n_0$ to $n = 0.95n_0$, where n_0 is the number density inside the bulk material.

Relating N_b (number of boundary atoms) to the surface area of the boundary, A_b, one obtains the number of atoms per surface area: $n_{bA} = N_b/A_b$. Assuming a discontinuous (step) density profile ($n = 0$ for $x < x_b$, $n = n_0$ for $x > x_b$) at the position, x_b, of the boundary, the interaction depth can be defined for a single atomic species as $d = n_{bA}/n_0$. Assuming that the atoms are arranged in an ordered fashion, the interaction depth can also be expressed in the form of atomic layers (atomic planes):

$$N_l = \frac{n_{bA}}{(n_0)^{2/3}} = d n_0^{1/3}, \tag{1}$$

where N_l is the interaction depth of the atomic layers.

For low-density gaseous media, it is possible to derive a theoretical expression for the relaxation zone width by balancing the kinetic energy of the atoms in 1D with the energy field that is generated by the external force, F^{ext}. The Boltzmann distribution [12],

$$f(E) = A\, e^{-(E/k_B T)}, \tag{2}$$

gives the probability for an atom to have the energy E in one degree of freedom. In the cases of a gas, the energy is represented by the kinetic energy defined by the velocity in the x-direction (perpendicular to the boundary). The factor A normalises the integral of (2).

The external force generates a potential energy field within the relaxation zone. In the direction normal to the boundary surface, the potential energy is $E_p(x) = (F_x^{ext}/N_b)x$, where x is the distance from the boundary (located at x_b) and F_x^{ext} is the external force acting in the x-direction. The distance an atom will travel against the external force depends on its kinetic energy in the x-direction. Thus, substitution of the potential energy into (2) gives the number density distribution within the relaxation zone:

$$n_{model}(x) = A\, e^{-(F^{ext}/N_b k_B T)x}. \tag{3}$$

The normalisation factor A is determined by the condition that, at $x = 0$ (start position of the relaxation zone), the number density is $n_{model}(x) = 0.95n_0$. Since for static cases, F_x^{ext} arises purely from the static pressure, it can be replaced by $F_x^{ext} = PA_b$. The density profile at the boundary can then be written as:

$$n_{model}(x) = 0.95 n_0\, e^{-(PA_b/N_b k_B T)x}. \tag{4}$$

From (4), the width of the relaxation zone is given by:

$$\delta l_b = \frac{N_l n_0^{2/3} k_B T}{P} \ln\frac{0.05}{0.95}. \tag{5}$$

The constant (ln(0.05/0.95)) emerges from the above definitions of the relaxation zone width (from $n = 0.05n_0$ to $n = 0.95n_0$). Note that this model neglects interatomic collisions and is, therefore, only applicable to cases in which δl_b is not significantly larger than the molecular mean free path.

2.3 Set-up and simulation procedure

To investigate the dependency of the relaxation zone width, δl_b, on the interaction depth, a series of simulations were performed to calculate δl_b for the range of interaction depths ($N_l = \{0.1, \ldots, 10\}$) both for low-density (gaseous state: $n_0 = 0.1$, $T = 2$) and high-density (liquid state: $n_0 = 0.8$, $T = 1$) cases. The influence of the temperature on δl_b was investigated by repeating the simulations for the high-density case with a higher temperature (super-critical state: $n_0 = 0.8$, $T = 2$). Finally, the dependence of δl_b on the number density was investigated for $n_0 = \{0.001, \ldots, 1\}$ and $N_b = 100$. The static pressure of the selected systems has been calculated through simple equilibrium simulations of bulk material in conjunction with periodic boundary conditions.

As illustrated in Figure 1, the boundary conditions were applied from the negative x-direction ($\alpha = x$). In the positive x-direction, the system was confined by a reflecting wall. For all simulations, periodic boundary conditions were applied in the y- and z-directions. An equilibration was performed over 50,000 time steps with $\delta t = 0.005$. Velocity scaling was applied to settle the temperature at the desired value, i.e. $T = 1$ or $T = 2$. Following stabilisation of the density profile at the boundary, the density profiles were time-averaged for each case over 100,000 time steps by using a 1D mesh in the x-direction. The calculations were performed every 100 time steps and averaged over 1000 samples.

3. Results

The density profiles for the gaseous case, with $n_0 = 0.1$, are plotted in Figure 2. To achieve a better comparison, the profiles are shifted so that the density values of $n = 0.95n_0$ coincide at $x_b = 0$. The measured density profiles fit well to the theoretical model (4) prediction, showing a sharp decrease from the bulk value followed by an asymptotic variation to zero value. Obviously, for larger N_b, the width of the relaxation zone increases, because the density function drops more slowly.

The corresponding density results for a liquid with $n_0 = 0.8$ and temperature $T = 1$ are presented in Figure 3.

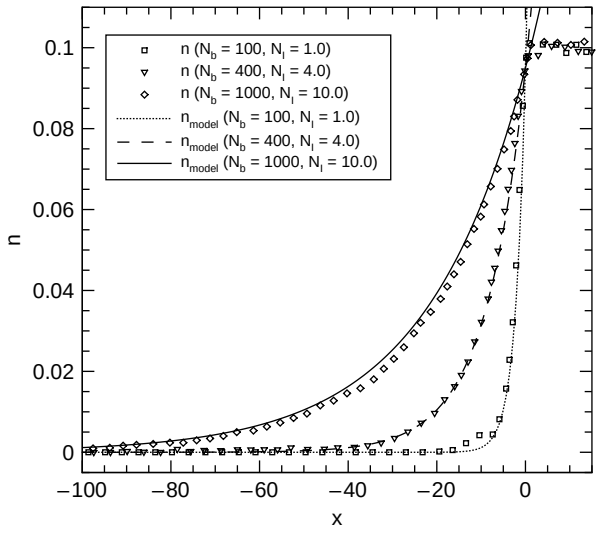

Figure 2. The number density profile across the relaxation zone for a set of interaction depths: $N_l = \{1, 4, 1\}$. The bulk material is in gaseous state with a number density of $n_0 = 0.1$ and temperature of 1.

Comparing these results with those for a gas, it is obvious that there is no abrupt density drop, starting from $n \approx n_0$. Instead, one can see a smooth transition to a linear region, followed by an asymptote to zero. For small N_b, the liquid density profiles show an oscillatory behaviour near x_b, which resembles the density variation of solid materials. In fact, very low interaction depths tend to resemble to a reflecting wall and, therefore, impose a crystal-like structure onto the liquid at the boundary. Note that (4) cannot model the density profile for the liquid case because it predicts a sharp decrease at x_b instead of the smooth transition observed in Figure 3. The origin of the smooth transition can be found in the attractive interatomic forces between the individual atoms, which cause energy transfers that are not accounted for by the model. Therefore, the number density profiles predicted by the model are not included in the plot. For the supercritical state ($n_0 = 0.8, T = 2$), the situation is similar to the liquid one. The number density profiles are shown in Figure 4. A smooth transition near $x_b = 0$ can be seen for higher values of N_l and oscillations for small values of N_l.

One question to address is how does the width of the relaxation zone change depending on the interaction depth? From (5), one expects the relaxation zone width δl_b to depend linearly on the interaction depth, at least for gaseous states. In Figures 5 and 6, δl_b is plotted over the interaction depth in the atomic layers, N_l, for different states. The complete plot, over the entire N_l range, in Figure 5 shows a good agreement between (5) and the measured relaxation zone widths for the three investigated states. In the gaseous case ($n = 0.1, T = 2$), the prediction only fails for very low values (Figure 6) of N_l ($N_l < 0.5$), where the measured values are higher than the ones predicted by the linear model (5). The relaxation widths are also well predicted for the liquid ($n = 0.8, T = 1$) and supercritical state ($n = 0.8,\ T = 2$). This is particularly interesting since the model was derived for a gas. The curve for the supercritical state fits very well over the entire investigated range. In the liquid case, the measured values are higher than the predicted ones for $N_l < 6$ and lower for $N_l > 6$. The reason for the good agreement of theoretical prediction of (5) with the results for the liquid

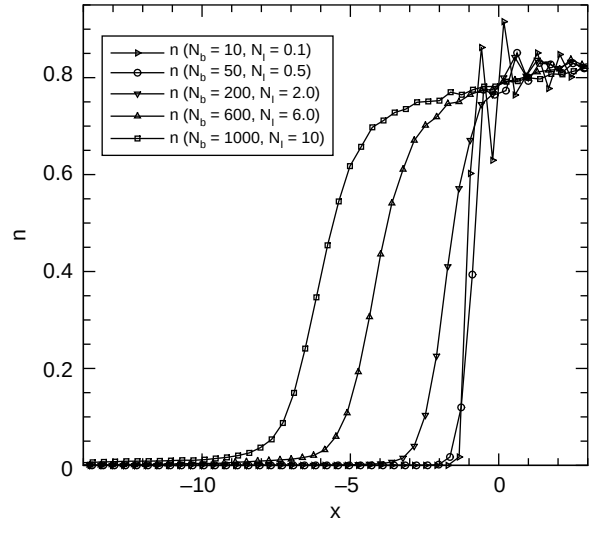

Figure 3. The number density profile across the relaxation zone for a set of interaction depths: $N_l = \{0.1, 0.5, 2.0, 6.0, 10.0\}$. The bulk material is in a liquid state with a number density of $n_0 = 0.8$ and temperature of 1.

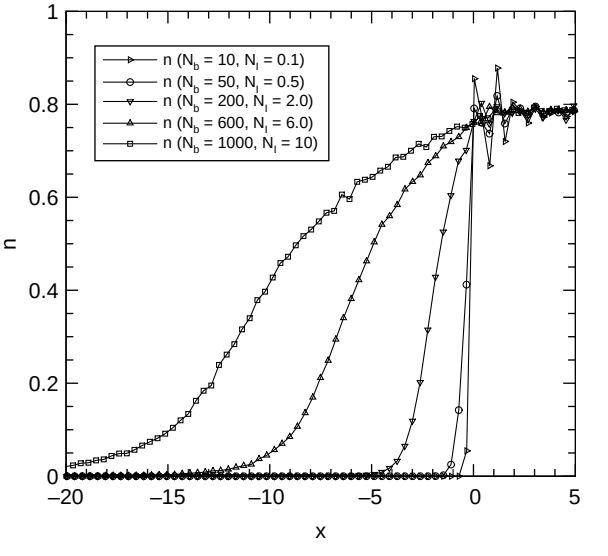

Figure 4. The number density profile across the relaxation zone for a set of interaction depths: $N_l = \{0.1, 0.5, 2.0, 6.0, 10.0\}$. The bulk material is in a supercritical state with a number density of $n_0 = 0.8$ and temperature of 2.

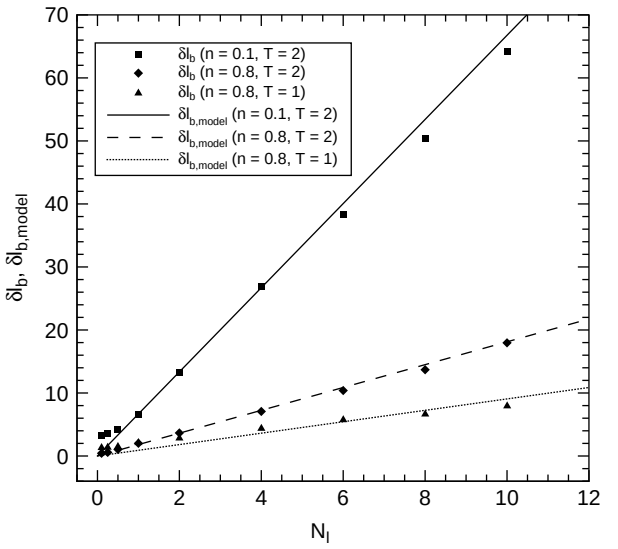

Figure 5. Relaxation zone width, δl_b, over interaction depth in atomic layers, N_l (complete view).

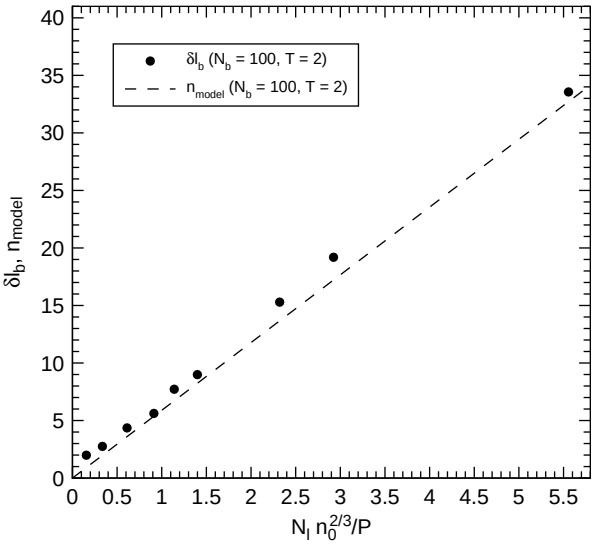

Figure 7. Relaxation zone width, δl_b, over $n_0^{2/3}/P$ for $N_b = 100$.

state is probably due to the relatively low surface tension of the LJ fluid. For liquids with more cohesive forces, such as water, the effects of surface tension would need to be incorporated into the model.

On the other hand, the proposed model can be expected to be applicable also for other particle methods, where the particles' velocity distribution is close to the Maxwell distribution function, as in dissipative particle dynamics (DPD) [8] and multiscale simulation methods [4] that use coarse-grained type potentials.

Another interesting question is how does the relaxation zone width change for different densities? According to (5), δl_b must be proportional to $n_0^{2/3}/P$. Figure 7 shows that this is indeed the case for the series of calculations, performed here with $N_b = 100$ for a range of number densities, $n_0 = \{0.001, \ldots, 1\}$. The measured values are only slightly higher than the predicted ones.

Finally, the results of all performed simulations are compared in Figures 8 and 9, where δl_b is plotted against the term $N_l n^{2/3} T/P$. According to (5), the measured values for δl_b should lie along the theoretical line, which is denoted by a solid line in Figures 8 and 9. This is true for all the investigated series of $N_l n^{2/3} T/P$ values larger than 1. The series that aligns best with the predictions is the one of

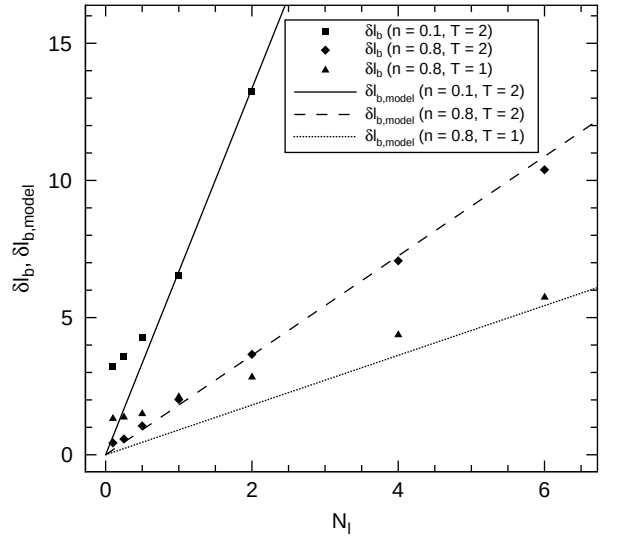

Figure 6. Relaxation zone width, δl_b, over interaction depth in atomic layers, N_l (magnified view).

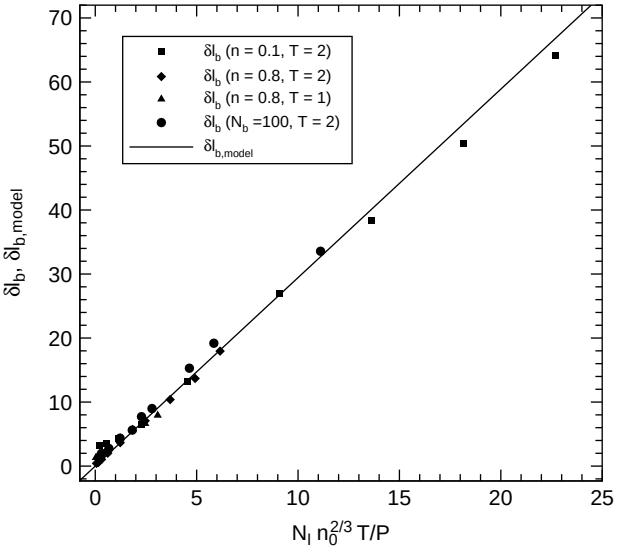

Figure 8. Relaxation zone width, δl_b, over $N_l n^{2/3} T/P$ (linear scale).

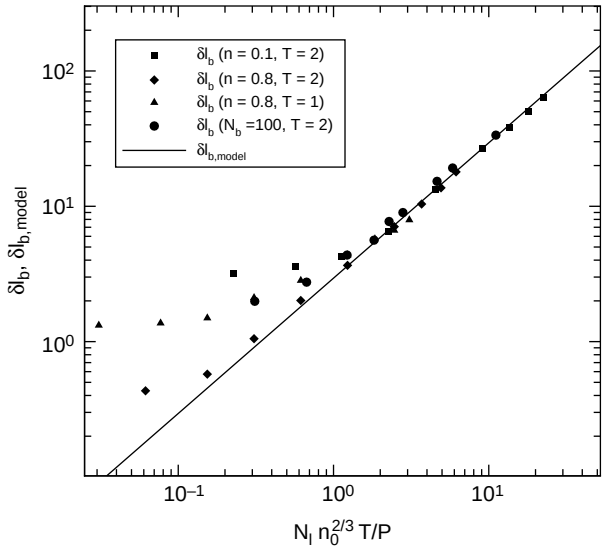

Figure 9. Relaxation zone width, δl_b, over $N_l n^{2/3} T/P$ (logarithmic scale).

the supercritical state, for which the measured values of δl_b follow the theoretical line even for values of $N_l n^{2/3} T/P$ less than 1. The other series show deviations for $N_l n^{2/3} T/P < 1$. Note, however, that the deviations in Figure 9 appear particularly large due to the logarithmic scale. On the linear scale, these deviations are almost unnoticeable.

4. Conclusions

An investigation of the density profile of fluidic material confined by a force field, as occurs across the boundaries of molecular domains used in (multiscale) hybrid MD-CFD simulations, was performed for LJ fluids in gaseous, liquid and supercritical states. It was found that the interaction depth in the atomic layers, N_l, is the most suitable parameter to describe the number of atoms, onto which the external force is applied to. The relaxation zone width, δl_b, increases with increasing interaction depth. Figures 2–4 provide an estimation of how many boundary atoms should be used for an LJ fluid in order to obtain a small relaxation zone without causing numerical artefacts. A value of $N_l \approx 2$ for gaseous and supercritical states, and $N_l \approx 5$ for the liquid state seem to be practical choices. The density profile for the gaseous state is well described by the theoretical model (4). Furthermore, the relaxation zone width, δl_b, is well predicted by (5) for the investigated gaseous, liquid and supercritical states. The present theoretical model can be used for estimating the characteristics of the relaxation zone in MD simulations, which make use of external forces to confine the fluidic material within the molecular domain. Furthermore, the model is expected to be applicable to DPD methods as well.

Acknowledgements

The financial support from the Engineering and Physical Sciences Research Council (EP/D051940/1), the MoD-AWE Joint Grant Scheme (JGS 607) and the EU project DINAMICS is greatly appreciated.

References

[1] M.P. Allen and D.J. Tildesley, *Computer Simulation of Liquids*, Oxford University Press, Oxford, 1987.
[2] R. Delgado-Buscalioni and P.V. Coveney, *Continuum-particle hybrid coupling for mass, momentum and energy transfers*, Phys. Rev. E 67 (2003), p. 046704.
[3] R. Delgado-Buscalioni, G. De Fabritiis, and P.V. Coveney, *Multiscale modeling of liquids with molecular specificity*, Phys. Rev. Lett. 97 (2006), p. 036709.
[4] R. Delgado-Buscalioni, K. Kremer, and M. Praprotnik, *Concurrent triple-scale simulation of molecular liquids*, J. Chem. Phys. 128 (2008), p. 114110.
[5] D. Drikakis and M. Kalweit, *Computational modelling of flows and mass transport processes in nano-technology*, in *Handbook of Computational Nanotechnology*, M. Rieth, and W. Scommers, eds., American Scientific Publishers, Stephenson Ranch, CA, 2006.
[6] G.D. Fabritiis, M. Serrano, R. Delgado-Buscalioni, and P.V. Coveney, *Fluctuating hydrodynamic modelling of fluids at the nanoscale*, Phys. Rev. E 75 (2007), p. 026307.
[7] E.G. Flekkoy, G. Wagner, and J. Feder, *Hybrid model for combined particle and continuum dynamics*, Europhys. Lett. 52 (2001), pp. 271–276.
[8] P.J. Hoogerbrugge and J.M.V.A. Koelman, *Simulating microscopic hydrodynamic phenomena with dissipative particle dynamics*, Europhys. Lett. 19 (1992), pp. 155–160.
[9] M. Kalweit and D. Drikakis, *Multiscale methods for micro/nano flows and materials*, J. Comput. Theor. Nano Sci. 5 (2008), pp. 1923–1938.
[10] S.J. Plimpton, *Fast parallel algorithms for short-range molecular dynamics*, J. Comput. Phys. 117 (1995), p. 1; available at http://www.lammps.sandia.gov.
[11] T. Werder, J. Walther, and P. Koumoutsakos, *Hybrid atomistic-continuum method for the simulation of dense fluid flows*, J. Comput. Phys. 205 (2005), pp. 373–390.
[12] G. Woan, *The Cambridge Handbook of Physics Formulas*, Press Syndicate of the University of Cambridge, Cambridge, 2000.